IEEE Access
Multidisciplinary | Rapid Review | Open Access Journal

Date of publication xxxx 00, 0000, date of current version xxxx 00, 0000.

Digital Object Identifier 10.1109/ACCESS.2022.Doi Number

Optimal Design of an IPMSM for HEVs Using Circular Area Movement Optimization with the Pattern Search Method

Joo-Chang Lee[1], and Dong-Kuk Lim[1]

[1] Department of Electrical, Electronic, and Computer Engineering, University of Ulsan, Ulsan 44610, Republic of Korea

Corresponding author: Dong-Kuk Lim (e-mail: ldk8745@ulsan.ac.kr)

This work was supported in part by the ''Regional Innovation Strategy (RIS)'' through the National Research Foundation of Korea (NRF) funded by the Ministry of Education (MOE) under Grant 2021RIS-003, and in part by the NRF Grant funded by the Korea Government (MSIT) under Grant 2022R1A2C2092905.

ABSTRACT In this paper, circular area movement optimization (CAMO), a novel global search algorithm, and its hybridization with the pattern search method (PSM) are proposed to solve the multimodal optimization problem. The CAMO is an optimization technique that creates a circular search area, moves the area, and searches the entire search area. Depending on the type of samples inside the area, two strategies are used to quickly and efficiently find the optimal point across the area. Also, the hybridization with the PSM supports fast convergence on adjacent optima from the points that are discovered in the global search using the CAMO. The effectiveness of the algorithm was verified by applying the CAMO to two test functions, and its superiority was confirmed through comparison with existing optimization algorithms. In addition, by applying the proposed algorithm to the optimal design of the cogging torque of an interior permanent magnet synchronous motor for a hybrid electric vehicle, a design that reduces the cogging torque by 95.65% was successfully derived. Lastly, stress analysis and demagnetization analysis were performed to examine the structural and thermal stability of the motor.

INDEX TERMS hybrid electric vehicle (HEV), interior permanent magnet synchronous motor (IPMSM), multi-modal optimization, pattern search method (PSM).

I. INTRODUCTION

Recently, due to the influence of environmental and energy regulations, the automobile industry is replacing conventional internal combustion engine (ICE) driven vehicles with eco-friendly vehicles such as electric vehicles (EVs), hybrid EVs (HEVs), and plug-in HEVs [1], [2]. HEVs utilize a motor during the start-up phase and at low speeds, while an ICE powers the vehicle at high speeds [3], [4]. This combination results in high energy efficiency [5], [6]. Given the need for high efficiency and high-power density in HEVs, interior permanent magnet synchronous motors (IPMSMs) that use rare earth permanent magnets are predominantly employed [7], [8]. When designing an IPMSM used to drive an EV or HEV, various factors such as torque ripple, average torque, and efficiency must be considered [9], [10]. However, in the design of IPMSMs, some output characteristics have correlations between variables, and the output performance responds in various ways according to changes in design variables, making it difficult to derive an optimal design that meets the desired performance [11]. A variety of methods are being studied to solve these problems, and the combination of optimization algorithms and finite element analysis (FEA) offers advantages over other methods in confirming the accurate electrical characteristics of the motor. However, it entails a significant amount of computational time. Hence, diverse studies are underway to reduce the analysis time [12], [13], [14], [15].

In this paper, a hybridization of circular area movement optimization (CAMO), a new global search algorithm, and pattern search method (PSM) is proposed to solve multimodal optimization problems. The CAMO finds the best solution candidates by creating and moving new circular areas across the entire problem domain and repeating this process to search the entire region to find various best solution candidates. The final optimal solution is derived by applying the PSM, a deterministic optimization method, to the optimal solution candidates obtained through the CAMO. The validity of the

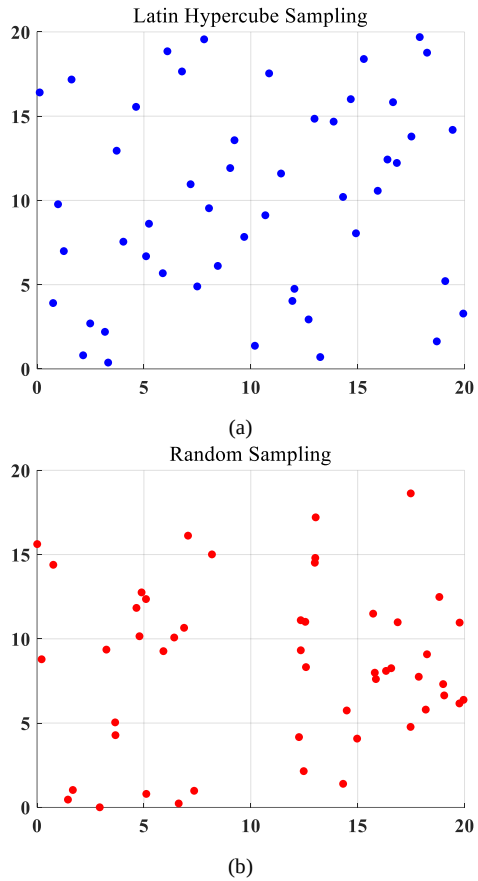

FIGURE 1. Comparison of sample distributions. (a) Latin hypercube sampling. (b) Random sampling.

proposed algorithm was verified by applying it to two test functions, and the performance was compared with the conventional algorithm, the niching genetic algorithm (NGA) [16]. Lastly, the proposed algorithm was applied to minimize the cogging torque of an IPMSM for an HEV. Additionally, stress analysis and irreversible demagnetization analysis were performed to ensure that structural stability and output performance were maintained.

II. CAMO WITH PSM

To effectively perform the hybrid algorithm, it is important to share the roles of the global and local search algorithms [17]. Therefore, in this paper, the CAMO is performed to explore the entire search region, and then the PSM is performed to find the optimal point quickly and accurately.

A. SAMPLING AND SAMPLE CLASSIFICATION

Since the proposed algorithm distinguishes the types of samples through the results of initial sampling and takes different search strategies depending on the types, it is important to generate samples evenly across the entire problem domain at this stage. Therefore, latin hypercube sampling (LHS), a uniform distribution method that considers the distance between each sample, is used [18]. LHS partitions each dimension (process parameter) into N separate, equal probability parts and then draws samples from each part according to the probability density of the random variables in that part. The samples are then randomly permuted to form a set of N d-dimensional samples, ensuring uniform coverage in each dimension [19]. Fig. 1 (a) and (b) show the results of sampling x and y in the [0, 20] interval through LHS and random sampling. As shown in Fig. 1, LHS samples more evenly across the area compared to random sampling.

TABLE I
PERFORMANCE COMPARISON ACCORDING TO K

Test function 1 (11 peaks)	Function-calls	Number of peaks found
k = 0.1	1957	11
k = 0.3	1700	11
k = 0.5	1226	11
k = 0.7	1216	3
k = 0.9	1212	1

A reference value is set to distinguish between good and bad samples among the samples generated by LHS. At this time, the reference value R is determined by multiplying the average fitness value among the initial sampling results by k, a value that exists between 0 and 1. The formula for determining the reference value is as follows:

$$R = k \cdot \max(f(x_1), f(x_2), ..., f(x_n)), \quad 0 < k < 1 \qquad (1)$$

where n is the number of samples and $f(x_n)$ denotes an objective function value of the n^{th} sample. In the proposed algorithm, the higher the value of k, the fewer the number of function calls, but the accuracy decreases, and some peaks are missed. On the other hand, as the value of k is set lower, the number of function calls increases, leading to improved accuracy and the generation of optimal solution candidates near all peaks. Table I shows the function calls for different values of k along with the number of peaks identified within the test function, which consists of 11 peaks. For k values of 0.5 or less, as k increases, all peaks are successfully identified and the number of function calls decreases. On the other hand, for k above 0.5, the number of function calls decreases slightly, but the number of peaks discovered decreases significantly. Therefore, in this paper, based on these results, k was set to 0.5 as the reference value.

B. CREATE A SEARCH AREA

Since the proposed algorithm has the characteristic of moving in the direction where good adjacent samples are located, it is likely to converge to the same optimal solution if an area is created near the optimal solution that has already been explored. In order to prevent this, when establishing a new area, we verify whether its center lies within the bounds of previously created areas by comparing their distances. The

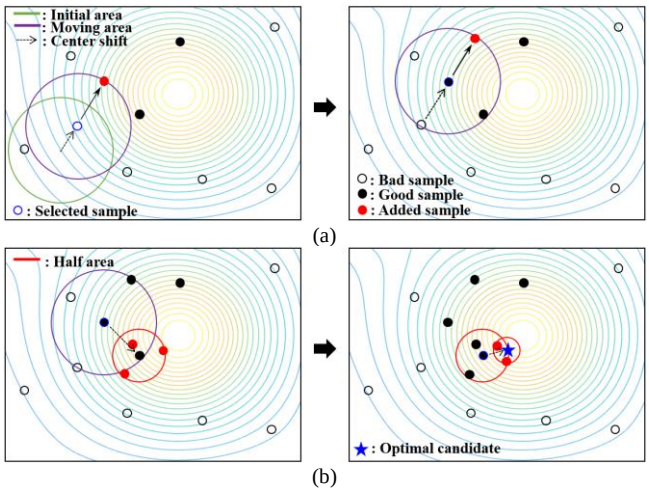

FIGURE 2. Concept of CAMO. (a) Case of good samples ≤ bad samples (b) Case of good samples > bad samples.

formula for calculating the distance is as follows:

$$r_{ri} = \sqrt{\sum_{i}^{n}\sum_{j=1}^{d}(x_{rij} - x_{ij})^2} \tag{2}$$

where r_{ri} represents the distance between the center of the newly formed area and the previously formed area. n and d correspond to the number of iterations and the dimension, respectively [20]. In addition, x_{ij} and x_{rij} represent the j^{th} coordinates of the previously created area and the newly formed area. If r_{ri} is less than the radius of the corresponding area, the area creation in cancelled, and area creation begins at another location. This process is repeated until the area to be newly created is not included in the existing generated area. If there is no sample inside the generated area, or if only one exists, the direction of movement cannot be determined, so the sample inside is added until there are more than two samples. The added sample is created on the opposite side of the existing sample and distributed evenly within the area.

C. MOVE SEARCH AREA

Movement methods are classified into two types depending on the type of sample that is more present in the area.

1) MORE BAD SAMPLES

If the number of bad samples in an area is greater than the number of good samples, the center of that area is moved to the best sample in that area. Afterwards, as shown in Fig. 2(a), the moving direction component of the center of the area is extracted, a sample is added at a point that has the same direction component as the extracted moving direction component and the displacement is equal to the radius, and the inclination with the sample inside the area is calculated from the center of the area. After calculation, the center moves in the direction with the largest slope value, and samples are added to the moving direction as before. In this case, if the slope is negative, it moves in the opposite direction. The formula for the slope is as follows:

$$d_i = \frac{f_0 - f_i}{\sqrt{\sum_{j=1}^{n}(x_{0j} - x_{ij})^2}} \tag{3}$$

where d_i denotes the slope, f_i denotes the objective function value of the i^{th} sample, and f_0 denotes the central objective function. The value x_{0j} is the coordinate of the j^{th} dimension of the center, and x_{ij} is the coordinate of the j^{th} dimension of the i^{th} sample. The number of bad samples and the number of good samples are compared again, and the process is repeated until there are more good samples in the area.

2) MORE GOOD SAMPLES

Similarly, if there are more good samples within that area, the best sample within that area is selected. As shown in Fig. 2(b), a new area is created around the changed position with half the radius of the previous area. Next, the samples are moved to the new area and compared to the previous best sample. The best sample from that area is then selected again, and when the best sample changes, half of the previous area is regenerated, and the sample is moved. When samples move, they are moved by considering the distance between samples so that they are evenly distributed within the new area. Considering the calculation time, this process is repeated until the radius of the area becomes smaller than a certain value or the density of the sample within the area exceeds a certain level. If the optimal sample does not change during this process, the existing optimal sample is selected as the optimal candidate and the search is terminated.

D. PATTERN SEARCH METHOD

The algorithm ends when the number of generated circular areas exceeds a certain number. The PSM is applied to the optimal solution candidates obtained through the CAMO. The PSM is a deterministic optimization method that finds the optimal point through exploratory movement and pattern movement [21]. First, an exploratory movement is performed, then the movement pattern with the best value is found and pattern movement is performed using the given equation.

$$x_p^{(k+1)} = x^{(k)} + (x^{(k)} - x^{(k-1)}) \tag{4}$$

where $x_p{}^{(k+1)}$ is the pattern movement result, $x^{(k)}$ is the exploratory movement result, and $x^{(k-1)}$ is the reference point. The exploratory move is performed again with $x_p{}^{(k+1)}$ as the starting point. If there is no pattern with a good value in the exploratory movement, the process is repeated by reducing the movement interval, and if the movement interval is less than a certain value, the search is terminated. The operation of the PSM in the proposed algorithm is

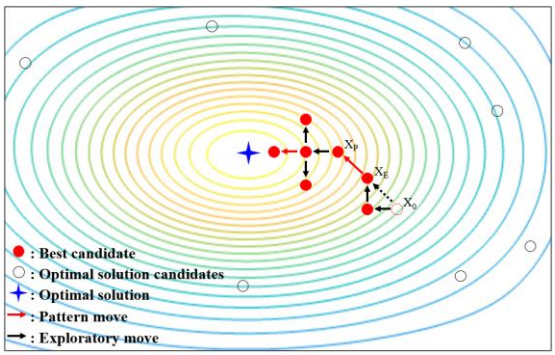

FIGURE 3. Concept of PSM.

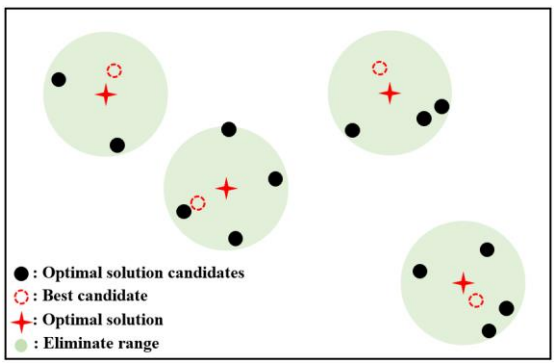

FIGURE 4. Concept of Eliminate optimal solution candidates.

shown in Fig. 3. The PSM is applied starting from the best optimal solution candidate to derive the optimal solution, and optimal solution candidates adjacent to the optimal solution have a high probability of converging to the same optimal point, therefore they are removed as shown in Fig. 4. The same process is repeated for the remaining optimal solution candidates, and the algorithm ends.

E. FLOWCHART

Fig. 5 shows the flowchart of the proposed algorithm. First, sampling is performed through LHS, and then the samples are divided into good and bad samples according to the reference value determined as a result of the sampling. After that, an area is created and the area is moved, sampling is performed within the area, and the area is finally moved near the optimal solution. At this time, two different strategies are used depending on the type and distribution of samples within the area. First, if the more bad samples, it can be judged that they are located far from the optimal point, therefore choose a strategy that can quickly move to the optimal point. On the other hand, the more good samples there are, the closer it can be to the optimal point, therefore selected a strategy that allows for accurate exploration. This process is repeated to evenly explore the entire problem domain, and then the PSM is applied to the derived optimal solution candidates.

III. VERIFICATION OF THE PROPOSED ALGORITHM

To verify the performance of the proposed algorithm, the CAMO was applied to two test functions with 11 peaks and

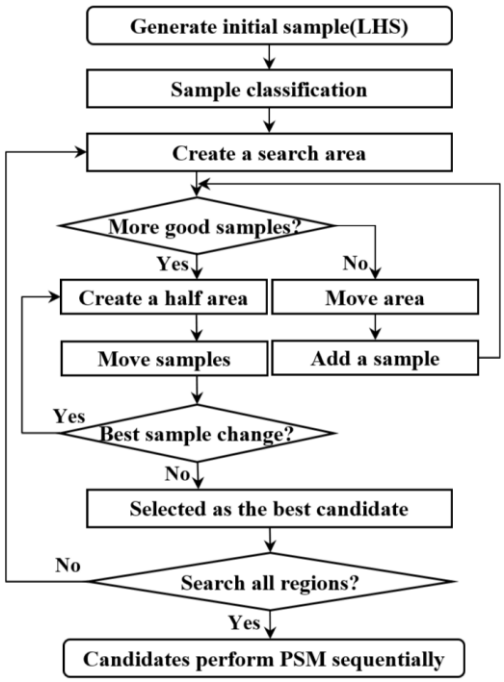

FIGURE 5. Flowchart of CAMO with PSM.

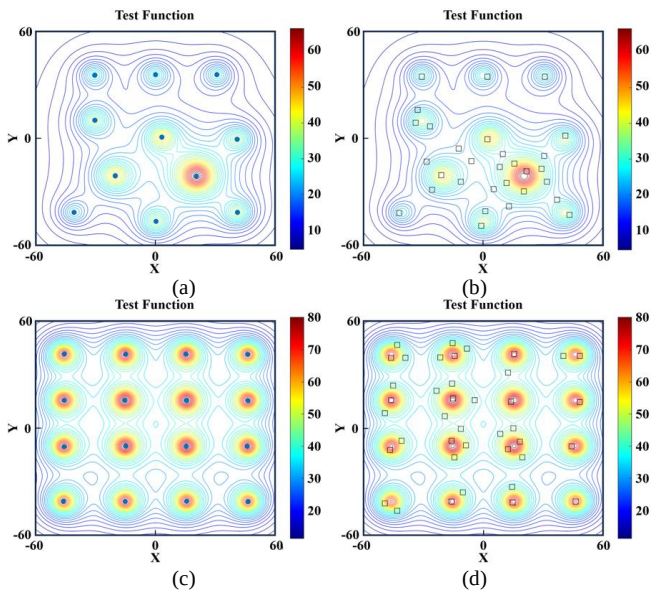

FIGURE 6. Result of Functions. (a) CAMO in function 1 (b) NGA in function 1 (c) CAMO in function 2 (d) NGA in function 2.

16 peaks and compared with the NGA a widely used conventional optimization algorithm that performs the same multimodal optimization as the proposed algorithm [22], [23], [24], [25]. The test function is as follows:

$$f(x,y)=\sum_{i=1}^{P}\frac{m_i}{1+[(x-x_i)^2+(y-y_i)^2]/n_i} \tag{5}$$

P is the number of peak points, and the height of the peak points is determined by m_i and n_i. The success rate was defined

TABLE II
PERFORMANCE COMPARISON OF CAMO AND NGA

Test function 1 (11 peaks)	Function-calls	Success rate [%]
CAMO	1226	99.48
NGA	1820	89.48
Test function 2 (16 peaks)	**Function-calls**	**Success rate [%]**
CAMO	1356	99.93
NGA	2040	85.19

as the ratio of the number of identified peaks to the actual number of peaks, and it was assumed that the peak was found when the difference between the actual peak value and the closest identified peak value was within 5%.

In test function 1 the CAMO achieved a success rate of 99.48% with 1,226 function calls, and the NGA had a success rate of 89.48% with 1,820 function calls. This result confirms that the CAMO required 32.64% fewer function calls and achieved an 11.18% higher success rate compared to the NGA. Similarly, in Test function 2, the CAMO achieved a success rate of 99.93% with 1,356 function calls, while the NGA had a success rate of 85.19% with 2,040 function calls. These results further validate that the CAMO required 33.53% fewer function calls and achieved a 14.74% higher success rate compared to the NGA.

IV. OPTIMAL DESIGN OF THE IPMSM

In order to examine whether the proposed algorithm can be applied to actual motor design, optimization of the HEV motor in Fig. 7 was performed using the algorithm, and the main specifications and output characteristics are summarized in Table III. In the case of the IPMSM, it has high-power density because it uses both reluctance torque and magnetic torque using magnetic salient polarity, but torque distortion such as cogging torque and torque ripple occurs due to this salient polarity [26]. The cogging torque that occurs at this time causes vibration and noise of the motor at the same time, causing discomfort to the user. In permanent magnet motors, cogging torque has a negative effect on motor operation, so cogging torque was selected as the objective function of the optimization algorithm [27], [28], [29]. According to [30], the formula for cogging torque can be expressed as follows:

$$T_{cog}(\alpha) = -\frac{\partial W}{\partial \alpha} = -\frac{\pi z L_{Fe}}{4\mu_0}(R_2^2 - R_1^2)\sum_{n=1}^{\infty} nG_{sn}B_{sn}\sin nz\alpha \quad (6)$$

where L_{Fe} is the axial length of the armature, R_1 is the outer radius of the rotor, R_2 is the inner radius of the armature, z is the number of slots, μ_0 is the permeability of air, and α is the rotor position. B_{sn} and G_{sn} are the Fourier expansion coefficients of the magnetic flux density by the permanent magnet and the permeability by the slot, respectively. Therefore, the cogging torque is determined by the shape of the rotor permanent magnet and the shape of the stator slot.

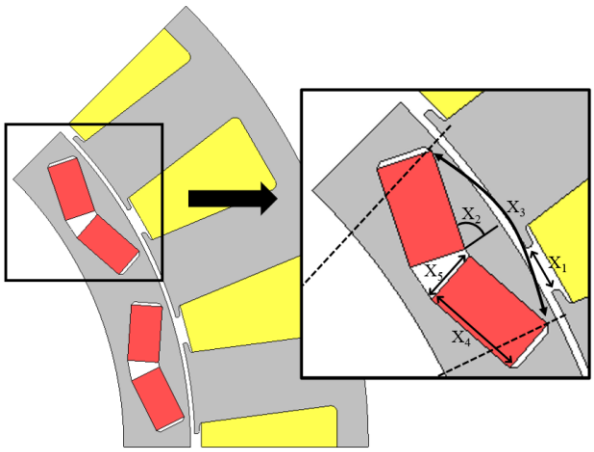

FIGURE 7. The 1/8 periodic analysis model of the initial model and design variables.

TABLE III
SPECIFICATIONS AND REQUIREMENTS

	Value
Pole / slot	16 / 24
Winding type	Concentrated winding
Stator inner / outer diameter [mm]	202 / 280
Rotor inner / outer diameter [mm]	170 / 200
Stacking length [mm]	70
Air gap [mm]	1.0
Bridge [mm]	1.2
Core material	35JN230
Permanent magnet	N39UH
Current density [A_{rms}/mm^2]	12
Rated output [kW]	52
Rated torque [Nm]	237
Rated speed [RPM]	2100

A. SENSITIVITY ANALYSIS

Cogging torque is affected by the shapes of the stator and rotor because it is generated by the interaction of permanent magnet magnetomotive force (MMF) harmonics and air gap permeance harmonics [31]. Therefore, a sensitivity analysis for cogging torque was performed for the stator and rotor shape design variables such as slot opening, magnet angle, pole arc to pole pitch ratio, magnet length, and magnet thickness, and were expressed as X_1, X_2, X_3, X_4 and X_5 respectively. The slot opening was limited to a minimum of 1mm considering manufacturability. The pole arc to pole pitch ratio, magnet angle, magnet length, and magnet thickness were limited in size so that the rotor shape could be created normally. The range of variables and the sensitivity analysis results are shown in Table IV. The sensitivity analysis used the Pearson correlation coefficient to determine the similarity between cogging torque values and design variables. The result has a value from -1 to 1. The larger the absolute value of the

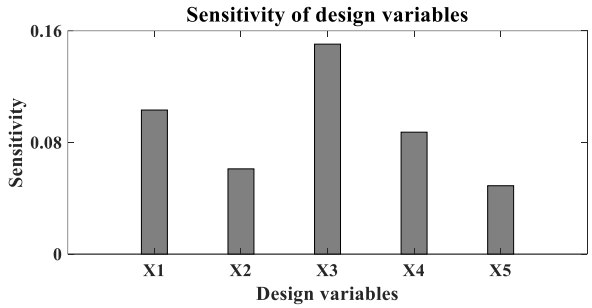

FIGURE 8. **Sensitivity analysis results for cogging torque.**

TABLE IV
RANGE OF DESIGN VARIABLES AND SENSITIVITY ANALYSIS RESULTS

Variables	Unit	Range	Sensitivity
X_1	mm	1 – 8	0.10
X_2	deg	65 – 80	0.06
X_3	none	0.65 – 0.80	0.15
X_4	mm	11.5 – 12.5	0.09
X_5	mm	5.5 – 6.5	0.05

correlation coefficient, the stronger the correlation, and the smaller the absolute value, the smaller the correlation [32].

$$\rho_{X,Y} = \frac{\mathrm{cov}(X,Y)}{\sigma_X \sigma_Y} = \frac{E((X-\mu_X)(Y-\mu_Y))}{\sigma_X \sigma_Y} = \frac{E(XY)-E(X)E(Y)}{\sqrt{E(X^2)-E^2(X)}\sqrt{B(Y^2)-E^2(Y)}} \quad (7)$$

where cov(*X*, *Y*) is the covariance between *X* and *Y* , and σ_X , σ_Y are the standard deviations of *X* and *Y*. *E(X)* is the expected value of *X*.

As shown in Fig. 8, as a result of the sensitivity analysis, X_1, X_2, X_3, X_4, and X_5 were derived as 0.10, 0.06, 0.15, 0.09, and 0.05. Therefore, X_1 and X_3, which showed high sensitivity were selected as design variables for the optimal design of the electric motor, and the cogging torque optimal design of the HEV traction motor was performed using the commercial software JMAG-Designer.

B. OPTIMAL DESIGN OF THE MOTOR

As a result of applying optimization to the motor design, three optimal model candidates were derived within the range of the design variables. First, the analysis results of the initial model showed that the cogging torque was 19.09 Nm, which was inferior to other electromagnetic characteristics. Next, comparing the optimization results, Model 1, Model 2, and Model 3 were found to be 1.54 Nm, 0.83 Nm, and 7.99 Nm, respectively. In terms of cogging torque, Model 2 has the best performance, and since Model 1 and Model 3 were also derived from the optimization results, it was confirmed that their cogging torque performance was better than the initial model. Meanwhile, since the relevant motor is an HEV driving motor, the average torque, torque ripple, and efficiency must

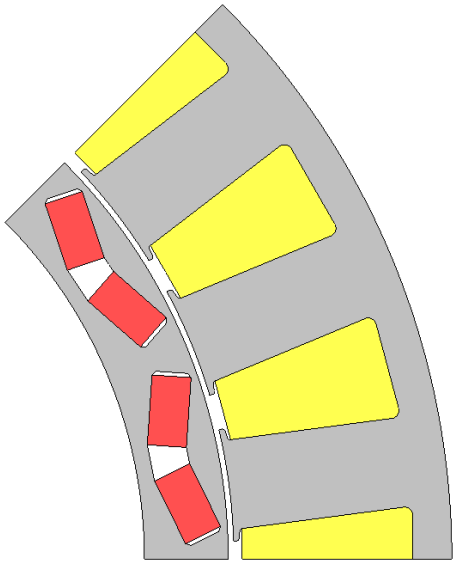

FIGURE 9. **The 1/8 periodic analysis model of the optimal model.**

TABLE V
OPTIMIZATION RESULT

Model	Initial	Model 1	Model 2	Model 3
X_1 [mm]	6.00	1.05	6.40	2.32
X_3	0.65	0.78	0.70	0.65
Cogging torque [Nm]	19.09	1.54	0.83	7.99
Average torque [Nm]	260.11	242.18	264.38	252.43
Torque ripple [%]	22.81	26.63	21.70	17.95
Efficiency [%]	96.48	96.18	96.53	96.34

be comprehensively considered [33]. Table V shows the cogging torque, average torque, torque ripple, and efficiency. Model 1 showed excellent cogging torque performance compared to the initial model, but the average torque was 242.18 Nm, the lowest among the optimized models and smaller than the initial model, and the torque ripple was also confirmed to be higher than the initial model at 26.63%. It was confirmed that the efficiency was also reduced to 96.18% compared to before. Next, Model 2 was confirmed to have the best cogging torque characteristics among the optimization candidate models, and the average torque and efficiency were the highest at 264.38 Nm and 96.53%, respectively, and the torque ripple was also found to be lower than the initial model at 21.70%. In the case of Model 3, the cogging torque characteristics were the worst among the three models, and the average torque and efficiency were confirmed to be smaller than the initial model at 252.43 Nm and 96.34%, respectively, but torque ripple was confirmed to be the best at 17.95%. Finally, Model 2 was selected as the optimal model by comprehensively considering the cogging torque, average torque, efficiency, and torque ripple. The shape of the final model is shown in Fig. 9.

The optimal model had a 95.65% reduction in cogging torque compared to the initial model, and an 4.87% reduction

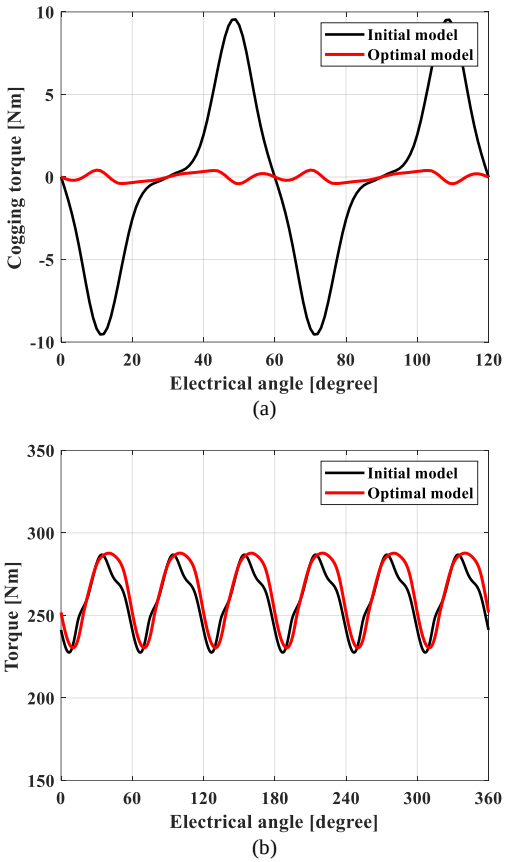

FIGURE 10. **Waveform comparison of the initial model and the optimal model. (a) Cogging torque. (b) Average torque.**

TABLE VI
PARAMETERS FOR THE MECHANICAL STRESS ANALYSIS

Parameter	Value
Young's modulus (core / magnet)	210 / 150 [GPa]
Poisson's ratio (core / magnet)	0.3 / 0.3
Density (core / magnet)	7600 / 7650 [Kg/m^3]
Yield stress	400 [MPa]
Maximum speed	5000 [RPM]
Reference safety factor	1.2

in torque ripple. Average torque increased by 1.26%, and efficiency also increased by 0.05%. Therefore, as a result of optimization, the overall electromagnetic characteristics have been improved compared to the initial model. Fig. 10 shows a comparison of the cogging torque and torque waveforms of the initial model and the optimal model.

C. STRESS ANALSYS

In general, the rotor structure design of an electric motor has a great influence on the electromagnetic and mechanical characteristics of the electric motor [34], [35]. There are many trade-offs between the electromagnetic performance and the mechanical performance of an electric motor. If the bridge is shortened to reduce the leakage flux of the electric motor, the

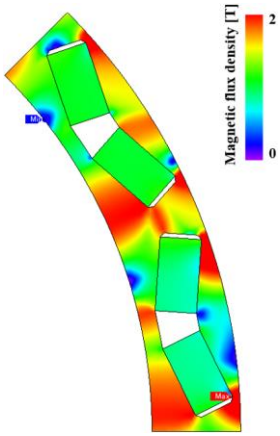

FIGURE 11. **Magnetic flux density contour plot of the rotor of the optimal model.**

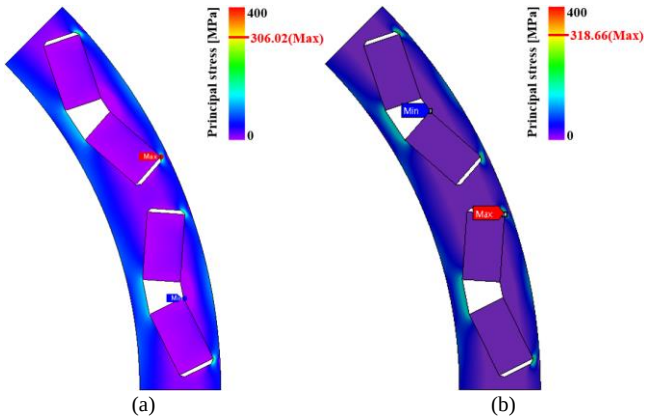

FIGURE 12. **Principal stress contour plot of the rotor of the optimal model. (a) JMAG-Designer. (b) ANSYS.**

mechanical strength of the rotor decreases [36]. Since the motor was designed by fixing the length of the bridge to 1.2 mm to reduce the amount of leakage of magnetic flux, stress analysis of the rotor was performed to review the mechanical stability of the rotor.

The stress analysis was performed at 6,000 RPM, 1.2 times the maximum speed, considering analysis errors. The physical properties of the rotor core and magnet are shown in Table VI. The results of the stress analysis were used to evaluate stability by calculating the safety factor, and the formula for calculating the safety factor is as follows:

$$\text{Safety factor} = \frac{\text{Yield stress}}{\text{Maximum stress}} \tag{8}$$

where the yield strength refers to the yield strength of the rotor steel plate, and the maximum stress refers to the maximum stress acting on the rotor. Fig. 11 and Fig. 12 show contour plots of magnetic flux density and stress acting on the rotor, respectively. In this paper, stress analysis was performed in the commercial software JMAG-Designer and ANSYS, respectively, to ensure the validity of the stress analysis.

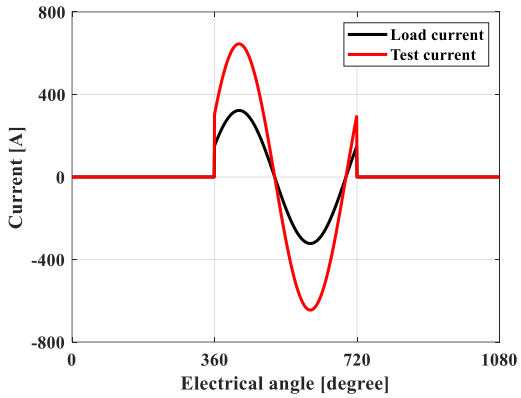

FIGURE 13. **Current waveform of the A-phase.**

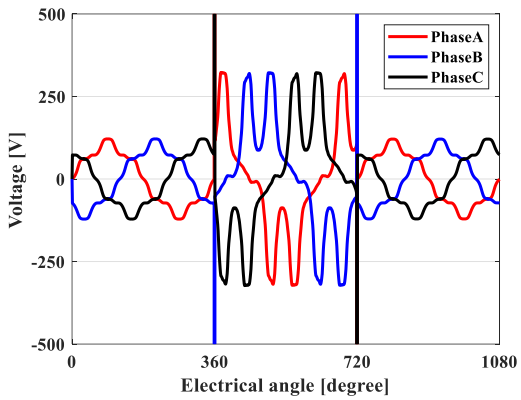

FIGURE 14. **Results of the irreversible demagnetization analysis by BEMF reduction rate at the high temperature.**

Through Fig. 11, it was confirmed that the bridge of the rotor was saturated, and the maximum stress of the rotor shown in Fig. 12 was confirmed to be 306.02 MPa in JMAG-Designer and 318.66 MPa in Ansys, respectively, which are small values compared to the yield strength of the Rotor steel plate, 400 MPa. The safety factors calculated through this were 1.31 and 1.26, respectively, which were higher than the standard safety factor of 1.2, confirming the structural stability of the electric motor. Additionally, the difference in analysis results between each software was 4.13%, confirming that the stress analysis was valid.

D. DEMAGNETIZATION ANALSYS

In the case of permanent magnets used in PMSM, irreversible demagnetization of the permanent magnet may occur due to armature reaction at high operating temperatures [37]. Irreversible demagnetization of permanent magnets can affect motor efficiency increase energy losses, and affect operational stability [38], [39], [40].

For this reason, a permanent magnet demagnetization analysis of the optimal model was performed. The demagnetization analysis was performed by checking the no-load back electromotive force at high temperature, applying a test current equal to twice the maximum current under load conditions as shown in Fig. 13, and then checking the no-load back electromotive force again and comparing the magnitude of the back electromotive force [41], [42].

As a result of performing the demagnetization analysis, it was confirmed that the output of the permanent magnet was maintained even at high temperatures, with the back electromotive force reduction rate being 0.41% under 150-degree operation conditions, as shown in Fig. 14. Through this, it was confirmed that the performance of the optimal model did not deteriorate even under high temperature operating conditions.

V. CONCLUSION

This paper proposes a hybridization of the CAMO and the PSM, a new global optimization algorithm to solve the multimodal optimization problem. The CAMO is an optimization technique that searches the entire problem area by moving the circular search area. It can evenly search the entire problem area but has the disadvantage of requiring many function calls to find the exact optimal point. Therefore, in this paper, the number of searches of the CAMO is limited, and an accurate optimal point is found with fewer function calls through combination with the PSM, a deterministic optimization method. The validity and superiority of the proposed algorithm were verified through comparison with the existing algorithm, NGA, and showed 11.18% higher accuracy with 32.64% fewer function calls based on test function 1. In addition, to apply the proposed algorithm to the IPMSM for HEVs, a sensitivity analysis was performed to select the design variables. As a result of applying the algorithm, cogging torque was reduced by 95.65% and torque ripple was also reduced by 4.87%. In addition, it was confirmed that the average torque was 264.38 Nm, achieving the required output characteristic of 237 Nm. Through this, the validity of the proposed algorithm was confirmed, and rotor stress analysis and permanent magnet demagnetization analysis were performed to examine the structural and thermal stability of the optimal model. As a result, structural stability was confirmed with a safety factor of 1.31, and the back electromotive force reduction rate was 0.41%, confirming that the permanent magnet maintains its performance even at high temperatures.

REFERENCES

[1] A. R. Salisa, N. Zhang and J. G. Zhu, "A Comparative Analysis of Fuel Economy and Emissions Between a Conventional HEV and the UTS PHEV," in IEEE Transactions on Vehicular Technology, vol. 60, no. 1, pp. 44-54, Jan. 2011.
[2] S. Shafiee, M. Fotuhi-Firuzabad and M. Rastegar, "Investigating the impacts of plug-in hybrid electric vehicles on power distribution systems", IEEE Trans. Smart Grid, vol. 4, no. 3, pp. 1351-1360, Sep. 2013.
[3] R. P. Joshi and A. P. Deshmukh, "Hybrid electric vehicles: The next generation automobile revolution", Proc. IEEE ICEHV, pp. 1-6, 2006-Dec.
[4] O. D. Momoh and M. O. Omoigui, "An overview of hybrid electric vehicle technology", Proc. 5th IEEE VPPC, pp. 1286-1292, 2009-Sep.
[5] Baoquan Kou, Liyi Li, Shukang Cheng and Fanrong Meng, "Operating control of efficiently generating induction motor for

driving hybrid electric vehicle," in IEEE Transactions on Magnetics, vol. 41, no. 1, pp. 488-491, Jan. 2005.
[6] F. Yan, J. Wang and K. Huang, "Hybrid Electric Vehicle Model Predictive Control Torque-Split Strategy Incorporating Engine Transient Characteristics," in IEEE Transactions on Vehicular Technology, vol. 61, no. 6, pp. 2458-2467, July 2012.
[7] J. -C. Son, J. -Y. Kim, J. -W. Choi, D. -K. Lim and H. -K. Yeo, "Performance Enhancement of the IPMSM for HEV Applications Using Grain Oriented Electrical Steel and Design Optimization," in IEEE Access, vol. 10, pp. 46599-46607, 2022.
[8] Y. -H. Hwang and J. Lee, "HEV Motor Comparison of IPMSM With Nd Sintered Magnet and Heavy Rare-Earth Free Injection Magnet in the Same Size," in IEEE Transactions on Applied Superconductivity, vol. 28, no. 3, pp. 1-5, April 2018.
[9] G. Hong, T. Wei and X. Ding, "Multi-Objective Optimal Design of Permanent Magnet Synchronous Motor for High Efficiency and High Dynamic Performance," in IEEE Access, vol. 6, pp. 23568-23581, 2018.
[10] C. Lu, S. Ferrari and G. Pellegrino, "Two Design Procedures for PM Synchronous Machines for Electric Powertrains," in IEEE Transactions on Transportation Electrification, vol. 3, no. 1, pp. 98-107, March 2017.
[11] D. Lee, S. Lee, J. W. Kim, C. G. Lee and S. Y. Jung, "Intelligent memetic algorithm using GA and guided MADS for the optimal design of interior PM synchronous machine," IEEE Trans. Magn., vol. 47, no. 5, pp. 1230–1233, May 2011.
[12] M. Sun, Y. Xu and K. Han, "Structure and Optimization Design of Cup Winding Permanent Magnet Synchronous Machine in Flywheel Energy Storage System," in IEEE Transactions on Magnetics, vol. 59, no. 5, pp. 1-5, May 2023.
[13] J. H. Lee, J. -W. Kim, J. -Y. Song, Y. -J. Kim and S. -Y. Jung, "A Novel Memetic Algorithm Using Modified Particle Swarm Optimization and Mesh Adaptive Direct Search for PMSM Design," in IEEE Transactions on Magnetics, vol. 52, no. 3, pp. 1-4, March 2016.
[14] Y. Wang, D. M. Ionel, V. Rallabandi, M. Jiang and S. J. Stretz, "Large-Scale Optimization of Synchronous Reluctance Machines Using CE-FEA and Differential Evolution," in IEEE Transactions on Industry Applications, vol. 52, no. 6, pp. 4699-4709, Nov.-Dec. 2016.
[15] D. Lee, J. -Y. Song, M. -K. Seo, H. -C. Jung, J. -W. Kim and S. -Y. Jung, "Development of Differing Extent Mesh Adaptive Direct Search Applied for Optimal Design of Spoke-Type PMSM," in IEEE Transactions on Magnetics, vol. 54, no. 11, pp. 1-5, Nov. 2018.
[16] E. Dilettoso and N. Salerno, "A self-adaptive niching genetic algorithm for multimodal optimization of electromagnetic devices," in IEEE Transactions on Magnetics, vol. 42, no. 4, pp. 1203-1206, April 2006.
[17] B. Son, G. -J. Park, J. -W. Kim, Y. -J. Kim and S. -Y. Jung, "Interstellar Search Method With Mesh Adaptive Direct Search for Optimal Design of Brushless DC Motor," in IEEE Transactions on Magnetics, vol. 52, no. 3, pp. 1-4, March 2016.
[18] C. -H. Wi and D. -K. Lim, "Tornado Optimization With Pattern Search Method for Optimal Design of IPMSM," in IEEE Transactions on Magnetics, vol. 58, no. 2, pp. 1-4, Feb. 2022.
[19] Jaffari and M. Anis, "On Efficient LHS-Based Yield Analysis of Analog Circuits," in IEEE Transactions on Computer-Aided Design of Integrated Circuits and Systems, vol. 30, no. 1, pp. 159-163, Jan. 2011.
[20] D. -W. Kim, G. -J. Park, J. -H. Lee, J. -W. Kim, Y. -J. Kim and S. -Y. Jung, "Hybridization Algorithm of Fireworks Optimization and Generating Set Search for Optimal Design of IPMSM," in IEEE Transactions on Magnetics, vol. 53, no. 6, pp. 1-4, June 2017.
[21] Y. -R. Kang, J. -C. Son and D. -K. Lim, "Optimal Design of IPMSM for Fuel Cell Electric Vehicles Using Autotuning Elliptical Niching Genetic Algorithm," in IEEE Access, vol. 8, pp. 117405-117412, 2020.
[22] Y. Jiang, Z. -H. Zhan, K. C. Tan and J. Zhang, "Optimizing Niche Center for Multimodal Optimization Problems," in IEEE Transactions on Cybernetics, vol. 53, no. 4, pp. 2544-2557, April 2023.
[23] Cheol-Gyun Lee, Dong-Hyeok Cho and Hyun-Kyo Jung, "Niching genetic algorithm with restricted competition selection for multimodal function optimization," in IEEE Transactions on Magnetics, vol. 35, no. 3, pp. 1722-1725, May 1999.
[24] B. Sareni, L. Krahenbuhl and A. Nicolas, "Niching genetic algorithms for optimization in electromagnetics. I. Fundamentals," in IEEE Transactions on Magnetics, vol. 34, no. 5, pp. 2984-2987, Sept. 1998.
[25] Sang-Yong Jung, Jae-Kwang Kim, Hyun-Kyo Jung, Cheol-Gyun Lee and Sun-Ki Hong, "Size optimization of steel-cored PMLSM aimed for rapid and smooth driving on short reciprocating trajectory using auto-tuning niching genetic algorithm," in IEEE Transactions on Magnetics, vol. 40, no. 2, pp. 750-753, March 2004.
[26] K. -C. Kim, "A Novel Method for Minimization of Cogging Torque and Torque Ripple for Interior Permanent Magnet Synchronous Motor," in IEEE Transactions on Magnetics, vol. 50, no. 2, pp. 793-796, Feb. 2014.
[27] W. Ren, Q. Xu, Q. Li and L. Zhou, "Reduction of Cogging Torque and Torque Ripple in Interior PM Machines With Asymmetrical V-Type Rotor Design," in IEEE Transactions on Magnetics, vol. 52, no. 7, pp. 1-5, July 2016
[28] I. -H. Jo, H. -W. Lee, G. Jeong, W. -Y. Ji and C. -B. Park, "A Study on the Reduction of Cogging Torque for the Skew of a Magnetic Geared Synchronous Motor," in IEEE Transactions on Magnetics, vol. 55, no. 2, pp. 1-5, Feb. 2019.
[29] Z. Li, X. Yu, X. Wang and X. Xing, "Optimization and Analysis of Cogging Torque of Permanent Magnet Spherical Motor," in IEEE Transactions on Applied Superconductivity, vol. 31, no. 8, pp. 1-5, Nov. 2021.
[30] D. Wang, X. Wang and S. -Y. Jung, "Cogging Torque Minimization and Torque Ripple Suppression in Surface-Mounted Permanent Magnet Synchronous Machines Using Different Magnet Widths," in IEEE Transactions on Magnetics, vol. 49, no. 5, pp. 2295-2298, May 2013.
[31] Z. Q. Zhu, S. Ruangsinchaiwanich, N. Schofield and D. Howe, "Reduction of cogging torque in interior-magnet brushless machines," in IEEE Transactions on Magnetics, vol. 39, no. 5, pp. 3238-3240, Sept. 2003.
[32] H. Zhu, X. You and S. Liu, "Multiple Ant Colony Optimization Based on Pearson Correlation Coefficient," in IEEE Access, vol. 7, pp. 61628-61638, 2019.
[33] Z. Yang, F. Shang, I. P. Brown and M. Krishnamurthy, "Comparative Study of Interior Permanent Magnet, Induction, and Switched Reluctance Motor Drives for EV and HEV Applications," in IEEE Transactions on Transportation Electrification, vol. 1, no. 3, pp. 245-254, Oct. 2015.
[34] K. Yamazaki and M. Kumagai, "Torque Analysis of Interior Permanent-Magnet Synchronous Motors by Considering Cross-Magnetization: Variation in Torque Components With Permanent-Magnet Configurations," in IEEE Transactions on Industrial Electronics, vol. 61, no. 7, pp. 3192-3201, July 2014.
[35] J. -W. Jung et al., "Mechanical Stress Reduction of Rotor Core of Interior Permanent Magnet Synchronous Motor," in IEEE Transactions on Magnetics, vol. 48, no. 2, pp. 911-914, Feb. 2012.
[36] F. Chai, Y. Li, P. Liang and Y. Pei, "Calculation of the Maximum Mechanical Stress on the Rotor of Interior Permanent-Magnet Synchronous Motors," in IEEE Transactions on Industrial Electronics, vol. 63, no. 6, pp. 3420-3432, June 2016.
[37] G. A. Skarmoutsos, K. N. Gyftakis and M. Mueller, "Detecting Partial Demagnetization in AFPM Generators by Monitoring Speed and EMF Induced in a Supplemental Winding," in IEEE Transactions on Industrial Informatics, vol. 18, no. 5, pp. 3295-3305, May 2022.
[38] J. Song, F. Dong, J. Zhao, H. Wang, Z. He and L. Wang, "An Efficient Multiobjective Design Optimization Method for a PMSLM Based on an Extreme Learning Machine," in IEEE Transactions on Industrial Electronics, vol. 66, no. 2, pp. 1001-1011, Feb. 2019.
[39] J. Song, J. Zhao, F. Dong, J. Zhao, L. Xu and Z. Yao, "A New Demagnetization Fault Recognition and Classification Method for DPMSLM," in IEEE Transactions on Industrial Informatics, vol. 16, no. 3, pp. 1559-1570, March 2020.
[40] J. Song, J. Zhao, F. Dong, J. Zhao and X. Song, "Demagnetization Fault Detection for Double-Sided Permanent Magnet Linear Motor Based on Three-Line Magnetic Signal Signature Analysis," in IEEE/ASME Transactions on Mechatronics, vol. 25, no. 2, pp. 815-827, April 2020.
[41] G. Jeong, H. Kim and J. Lee, "A Study on the Design of IPMSM for Reliability of Demagnetization Characteristics-Based Rotor," in IEEE

Transactions on Applied Superconductivity, vol. 30, no. 4, pp. 1-5, June 2020.

[42] T. Arakawa et al., "Examination of an Interior Permanent Magnet Type Axial Gap Motor for the Hybrid Electric Vehicle," in IEEE Transactions on Magnetics, vol. 47, no. 10, pp. 3602-3605, Oct. 2011.

JOO-CHANG LEE received the B.S. degree in electrical engineering from the School of Electrical Engineering, University of Ulsan, South Korea, in 2023, where he is currently pursuing the M.S.degree.

His research interest includes analysis and optimal design of electrical machines.

DONG-KUK LIM (Member, IEEE) received the B.S. degree in electrical engineering from Dongguk University, Seoul, South Korea, in 2010, and the Ph.D. degree in electrical engineering from Seoul National University, Seoul, in 2017, through the combined master's and Ph.D. program.

In 2017, he was a Senior Research Engineer with the Electrical Power Engineering Team, Hyundai Mobis Company, South Korea. He is currently an Associate Professor with the School of Electrical Engineering, University of Ulsan, South Korea. His research interest includes analysis and optimal design of electrical machines.